THE JOURNAL OF BIOLOGICAL CHEMISTRY VOL. 285, NO. 43, pp. 33540–33548, October 22, 2010

Multiple Decisive Phosphorylation Sites for the Negative Feedback Regulation of SOS1 via ERK*[S]

Received for publication, April 20, 2010, and in revised form, July 20, 2010 Published, JBC Papers in Press, August 19, 2010, DOI 10.1074/jbc.M110.135517

Yuji Kamioka[‡§1], **Shuhei Yasuda**[¶1], **Yoshihisa Fujita**[‡], **Kazuhiro Aoki**[¶‖], **and Michiyuki Matsuda**[‡¶2]

From the [‡]*Department of Pathology and Biology of Diseases, Graduate School of Medicine,* [¶]*Laboratory of Bioimaging and Cell Signaling, Graduate School of Biostudies, and* [§]*Innovative Techno-Hub for Integrated Medical Bio-Imaging, Kyoto University, Kyoto 606-8501 and* [‖]*Precursory Research for Embryonic Science and Technology, Japan Science and Technology Agency, Saitama 332-0012, Japan*

EGF-induced activation of ERK has been extensively studied by both experimental and theoretical approaches. Here, we used a simulation model based mostly on experimentally determined parameters to study the ERK-mediated negative feedback regulation of the Ras guanine nucleotide exchange factor, son of sevenless (SOS). Because SOS1 is phosphorylated at multiple serine residues upon stimulation, we evaluated the role of the multiplicity by building two simulation models, which we termed the decisive and cooperative phosphorylation models. The two models were constrained by the duration of Ras activation and basal phosphorylation level of SOS1. Possible solutions were found only in the decisive model wherein at least three, and probably more than four, phosphorylation sites decisively suppress the SOS activity. Thus, the combination of experimental approaches and the model analysis has suggested an unexpected role of multiple phosphorylations of SOS1 in the negative regulation.

EGF-induced activation of the ERK signaling pathway has a profound influence on many cellular processes, including proliferation, differentiation, and survival (1, 2). EGF first activates the EGF receptor (EGFR),[3] which recruits the Shc-Grb2-SOS complex to the plasma membrane (3). SOS is the primary guanine nucleotide exchange factor (GEF) that converts inactive Ras-GDP into active Ras-GTP in many EGF-stimulated cells (4). This Ras-GTP protein activates Raf at the cell membrane, which is followed by sequential activation of MEK and ERK. The activated ERK regulates more than 70 substrates, including nuclear transcription factors.

Dynamic control of the extent and kinetics of this EGF-ERK signaling is governed by positive and negative feedback loops. One example of the positive feedback regulation is a Ras-mediated increase in SOS GEF activity by an allosteric mechanism (5). A few examples of the negative feedback regulation include EGF receptor internalization mediated by Grb2, EGF receptor degradation induced by Cbl (for a review, see Ref. 6), and suppression of SOS GEF activity by ERK-mediated phosphorylation (7–9).

Several research groups have studied the role of growth factor-induced SOS phosphorylation but do not necessarily reach the same conclusion (7–12). Among the two SOS isoforms, SOS1 and SOS2, only SOS1 is phosphorylated by ERK (9). Growth factor-induced phosphorylation of SOS1 is mediated mostly by ERK, which phosphorylates at least four serine residues in the C-terminal region of SOS1 (8, 9, 12). All these previous studies agree with the negative regulation by ERK phosphorylation of SOS1, but the mechanism is controversial. In some studies, the phosphorylation of SOS1 is suggested to induce disassembly of the Grb2-SOS1 complex, thereby terminating SOS1-dependent Ras activation (9–11). However, in others, it is reported that the phosphorylation of SOS1 does not affect the binding of SOS1 to Grb2 but does induce dissociation of the Grb2-SOS complex from the activated EGF receptor (8, 12). Notably, in these previous studies, the role of multiplicity of phosphorylation sites has not been studied.

Kinetic simulation models have been increasingly used to clarify this complex network of the EGF-ERK signaling pathway (for a review, see Ref. 13). Each kinetic simulation model reported previously recapitulates the stimulus-induced ERK activation fairly well. Nevertheless, the parameters used therein are sometimes astonishingly different from each other (14). One apparent reason for this discrepancy is that these studies often use different algorithms to fit the parameters to the experimental data (15–17). Another reason may be that some parameters are derived from *in vitro* experiments, which may not reflect *in vivo* conditions. For these reasons, development of a kinetic simulation model using parameters collected in living cells or under physiological conditions is awaited as a solid basis for future theoretical studies.

To collect and evaluate the parameters in living cells, we previously adopted fluorescent protein technologies and developed a kinetic simulation model based on the experimentally validated parameters (14). This simulation model contained only four signaling molecules, Ras, Raf, MEK, and ERK, but still

* This work was supported by the Cell Innovation Program and Innovative Techno-Hub for Integrated Medical Bio-imaging Project from the Ministry of Education, Culture, Sports, Science and Technology, Japan; a Sagawa Cancer Research grant; the Japan Science and Technology Agency Precursory Research for Embryonic Science and Technology program; and the Kyoto University Global Center of Excellence Program Center for Frontier Medicine.

[S] The on-line version of this article (available at http://www.jbc.org) contains supplemental Tables S1–S3 and Figs. S1–S5.

[1] Both authors contributed equally to this work.

[2] To whom correspondence should be addressed: Laboratory of Bioimaging and Cell Signaling, Graduate School of Biostudies, Yoshida-Konoe-cho, Sakyo-ku, Kyoto University, Kyoto 606-8501, Japan. Fax: 81-75-753-4698; E-mail: matsudam@lif.kyoto-u.ac.jp.

[3] The abbreviations used are: EGFR, EGF receptor; SOS, son of sevenless; GEF, guanine nucleotide exchange factor; TFP, teal fluorescent protein; mTOR, mammalian target of rapamycin; CFP, cyan fluorescent protein; CCD, charge-coupled device; LDR, Lyn11-targeted FRB; FKBP, FK506-binding protein; EGFP, enhanced GFP; pSOS, phosphorylated SOS1; RB, retinoblastoma tumor suppressor protein.

successfully reproduced the essential features of the Ras-ERK MAPK pathway and demonstrated the usefulness of the parameters collected in living cells.

In this study, we have extended this approach to include SOS in this model. First, we confirmed the role of SOS phosphorylation in the negative feedback loop and examined the dephosphorylation rate in the cells. Second, the role of multiple phosphorylation sites was studied with the kinetic simulation models based on the experimentally validated parameters. We found that the multiple phosphorylation sites must independently and decisively suppress SOS GEF activity to reproduce the transient Ras activation.

EXPERIMENTAL PROCEDURES

Reagents—U73122, Gö6983, LY294002, SB203580, PP2, FR180204, and rapamycin were purchased from Calbiochem. EGF, U0126, puromycin, and blasticidin S were purchased from Sigma-Aldrich. Small interfering RNA (siRNA) oligonucleotide against human SOS1 (SI00079793) was purchased from Qiagen (Hilden, Germany). siRNA against human SOS2 (sense, 5′-GCCUUUGCUAGAAAAUGCAGAAACU-3′) was purchased from iGENE Therapeutics (Tsukuba, Japan). Stealth RNAi negative control duplex (Invitrogen) was used as a control siRNA. Anti-tubulin (Ab-1) was purchased from Calbiochem. Anti-SOS2 (sc-258) was purchased from Santa Cruz Biotechnology (Santa Cruz, CA). Anti-phospho-ERK (9101) and anti-phospho-EGFR (2236) were purchased from Cell Signaling Technology (Danvers, MA). Anti-SOS1 (610096), anti-phosphotyrosine (610000), and anti-ERK (610123) were pursed from BD Transduction Laboratories.

Cell Culture—HeLa cells were obtained from the Human Science Research Resources Bank (Sennan-shi, Japan) and maintained in DMEM (Wako Pure Chemical Industries, Osaka, Japan) supplemented with 10% fetal bovine serum and 1% penicillin-streptomycin solution (Invitrogen). BOSC23 cells were purchased from ATCC (Manassas, VA) and maintained in DMEM supplemented with 10% fetal bovine serum.

Stable Expression of FRET Probes by Retrovirus-mediated Expression—We previously reported the FRET probes for Ras activity and tyrosine kinase activity, Raichu and Picchu, respectively (18, 19). Retroviral expression plasmids for Raichu and Picchu were constructed as follows: cDNA for monomeric TFP (Allele Biotechnology, San Diego, CA) was PCR-amplified and substituted for cyan fluorescent protein (CFP). The cDNA of the TFP version of FRET probes was inserted into a retroviral vectors pCX4 (20) or pMCs (Cell Biolabs, San Diego, CA), to generate pCX4neo-Raichu-HRas and pMCsbsr-Picchu. Retroviruses for the FRET probes were produced in BOSC23 cells and inoculated into HeLa cells expressing the ecotropic retroviral receptor, EcoVR, as described previously (20). After selection with either G418 or blasticidin S, cells expressing a modest level of biosensors were isolated.

Rapamycin-inducible cRaf Translocation System—The rapamycin-inducible translocation system was constructed according to Inoue *et al.* (21); a schematic representation of this system is shown in Fig. 4*A*. The retroviral expression vector pMCsbsr-cRaf-FKBP encodes an FKBP-cRaf fusion protein consisting of the cRaf protein and the rapamycin-binding domain of FKBP12. The retroviral vector pCX4puro-LDR encodes a fusion protein consisting of the N-terminal myristoylation signal of Lyn and the FK506-rapamycin binding domain of mammalian target of rapamycin (mTOR). HeLa cells infected with retroviruses derived from pMCsbsr-cRaf-FKBP and pCX4puro-LDR were selected with 2.0 μg/ml puromycin and 10 μg/ml blasticidin S. Cells were stimulated with 50 nM rapamycin for 10 min and subjected to immunoblotting analysis.

Immunoblotting and Ras-GTP pulldown Assay—siRNA oligonucleotides were transfected with RNAi MAX (Invitrogen) according to the manufacturer's protocol. Other plasmids were transfected with 293Fectin (Invitrogen). Lysed cells were analyzed by SDS-PAGE followed by immunoblotting. Precast SDS-polyacrylamide gels were purchased from Wako Pure Chemical Industries or System Instruments (Tokyo, Japan). Immunoblotting was performed according to the protocols of each manufacturer of the antibodies. Bound antibodies were detected with secondary antibodies conjugated with IRDye680 or IRDye800 and analyzed with an Odyssey Imager system (LI-COR, Lincoln, NE). For detection of Ras-GTP, Bos and co-workers' (22) pulldown assay with the GST-tagged Ras-binding domain of cRaf was performed as described previously.

Quantification of EGFR and SOS1—Protein concentrations of the endogenous EGFR and SOS1 in HeLa cells were determined as described previously (14). First, serial dilutions of total HeLa cell lysates expressing EGFP-tagged EGFR and SOS1 and GST-tagged YFP were applied to the same SDS-polyacrylamide gels, transferred to PVDF membrane, and probed with anti-GFP antibody. The bound antibody was quantified with an Odyssey Imager system to plot a calibration curve. Second, the EGFP-EGFR and EGFP-SOS1 were used as the standard to quantify the endogenous EGFR and SOS1. Recombinant GST-tagged YFP was prepared in our laboratory (23). Expression plasmids for EGFR-EGFP and EGFP-mSOS1 were also prepared in our laboratory.

Imaging with FRET Probes—HeLa cells expressing FRET probes were plated on 35-mm glass-based dishes (Asahi Techno Glass, Tokyo, Japan), which were coated with collagen type I (Nitta Gelatin Inc., Osaka, Japan), and maintained in phenol red-free DMEM (Invitrogen). Before imaging, the medium was replaced with phenol red-free M199 medium (Invitrogen) containing 0.1% BSA and overlaid with mineral oil (Sigma-Aldrich) to prevent evaporation. The HeLa cells expressing FRET probes were imaged every 1 or 2 min with an Olympus IX81 inverted microscope equipped with a light-emitting diode light source PreciseExcite (CoolLED, Hampshire, UK), a CoolSNAP K4 cooled charge-coupled device (CCD) camera (Roper Scientific, Trenton, NJ), a laser-based autofocusing system (IX2-ZDC, Olympus), and an automatically programmable XY stage (MD-XY30100T-Meta, Sigma Koki, Tokyo, Japan), which allowed us to obtain time lapse images of several view fields in a single experiment. The imaging system was controlled by MetaMorph software (Universal Imaging, West Chester, PA). The filters used for the dual emission imaging were obtained from Omega Optical and consisted of an XF1071 (440AF21) excitation filter, an XF2034 (455DRLP) dichroic mirror, and two emission filters (XF3075 (480AF30) for CFP and XF3079

(535AF26) for FRET). Cell images were acquired with a 60× oil immersion objective lens (PlanApo 60×/1.4, Olympus). The binning of the charge-coupled device camera was 8. The exposure time was 100 ms for the TFP and FRET images. After background subtraction, FRET/TFP ratio images were created with MetaMorph software. Quantification of the time course of the FRET images was conducted according to Aoki and Matsuda (24).

Determination of Dephosphorylation Rate of SOS1—Upon EGF stimulation, SOS1 is phosphorylated at multiple serine residues, which is manifested by an electrophoretic mobility shift in SDS-PAGE (7–9). We quantified this band shift as follows. First, HeLa cells were starved for 3 h and stimulated with EGF for 10 min to maximize the SOS1 phosphorylation by ERK. Second, MEK activity was acutely ablated by U0126 treatment. After predetermined periods of incubation, cells were lysed for the SDS-PAGE and immunoblotting analysis. FLAG-tagged DOCK180 protein was added to the cell lysates as an internal molecular size marker (25). After separation in a 5% SDS-polyacrylamide gel, proteins were transferred to PVDF membrane and probed with anti-FLAG and anti-SOS1 primary antibodies and fluorescent dye-labeled secondary antibodies. The distance between FLAG-DOCK180 and SOS1 was measured for the band shift analysis. Third, we calculated the phosphorylation rate assuming that the level of band shift was linearly correlated with the multiplicity of phosphorylation. Here, we postulated that the concentration and activity of phosphatase(s) remained constant during the course of simulation. Thus, the production rate of unphosphorylated SOS1 was

$$\frac{d[SOS]}{dt} = \frac{k_{cat}\_phosphatase\_pSOS \times [phosphatase] \times [pSOS]}{K_m\_phosphatase\_pSOS + [pSOS]} \quad \text{(Eq. 1)}$$

where k_{cat}_phosphatase_pSOS and K_m_phosphatase_pSOS are the rate and the Michaelis constant of this phosphatase reaction, respectively. Assuming that phosphatase activity is constant and that K_m_phosphatase_pSOS is greatly larger than [pSOS], this reaction can be approximated by the first-order kinetics

$$\frac{d[SOS]}{dt} = \frac{V_{max}\_pSOS\_ \times [pSOS]}{K_m\_phosphatase\_pSOS} = k_d phos\_pSOS\_SOS \times [pSOS] \quad \text{(Eq. 2)}$$

where V_{max}_pSOS and $k_d$phos_pSOS_SOS are the maximum rate and the first-order rate constant, respectively. We obtained this first-order rate constant by fitting the dephosphorylation time course of SOS1 with a single exponential decay function using Excel Solver.

Simulation—The EGF-ERK pathway simulation implemented here consists of 27 kinetic reactions involving 10 different molecules and 33 parameters. Kinetic reactions were based on Michaelis-Menten kinetics, but many reactions were described as the first-order kinetics when reactions could be approximated to decrease the number of parameters. The biochemical reactions and the rate constants used in this study are shown in supplemental Tables S1 and S2 and supplemental Fig. S2. The simulation program described by using Cell Designer (Systems Biology Institute, Tokyo, Japan) was transferred to and run on MATLAB (MathWorks, Natick, MA).

RESULTS

Attenuation of EGF-induced Ras Activation by ERK in HeLa Cells—To analyze the negative feedback loop from ERK to Ras at the single cell level, we established a cell line expressing a FRET probe for Ras, Raichu-HRas (19). In this cell line, the concentration of the probe was 0.27 μM, which is about two-thirds that of the endogenous Ras proteins, 0.40 μM. As reported previously (13, 15, 30), EGF-induced Ras activation was transient due to feedback suppression but was sustained by pretreatment with an MEK inhibitor, U0126 (Fig. 1*A*), or ERK inhibitor, FR180204.[4] This observation was confirmed by a pulldown assay with the GST-tagged Ras-binding domain of cRaf (Fig. 1, *B* and *C*). On the other hand, the activity of EGFR tyrosine kinase, which was monitored with another FRET probe, Picchu (18), was not affected by U0126 pretreatment (Fig. 1*D*). Thus, the ERK-mediated negative feedback loop was found to enter the signaling cascade downstream of EGFR.

To exclude the possible off-target effect of U0126, we adopted two approaches. First, we knocked down MEK1 and MEK2 by siRNA (supplemental Fig. S1, A–C). Knockdown of MEK1 and MEK2 suppressed the rapid and transient activation of Ras within 5 min of EGF application. Notably, however, the weak Ras activation was prolonged as observed in U0126-treated cells. Although the cause of the suppression of Ras activation is unknown, this observation also supported that the presence of MEK and ERK mediated the negative feedback loop to Ras. We also examined the effect of another MEK inhibitor, PD184352, and obtained similar results (supplemental Fig. S1D).

Essential Role of SOS1 in EGF-dependent Ras Activation—We focused on SOS as the target of negative regulation. There are two isoforms of SOS, SOS1 and SOS2, in human cells. We depleted SOS1 and/or SOS2 and measured the EGF-induced Ras activation (Fig. 2). Depletion of SOS1 inhibited the EGF-induced Ras activation almost completely irrespective of the presence of SOS2, indicating that SOS1 was the primary GEF for Ras in EGF-stimulated HeLa cells. In contrast, the effect of SOS2 depletion was negligible. Therefore, we further focused on SOS1 in the following study. Notably, Ras activity was decreased rapidly and transiently in the SOS1 and SOS2 knockdown cells, suggesting EGF stimulation of GTPase-activating protein(s) for Ras, for example GAP1m (26). Because this decrease in Ras activity continues less than 4 min, we neglected this potential activation of GTPase-activating protein(s) in this study, which focuses on the role of SOS1 phosphorylation in the later phase, *i.e.* from 10 to 30 min after EGF stimulation.

ERK-dependent Phosphorylation of SOS1—It has been shown that SOS1 phosphorylation causes retardation of electrophoretic mobility in an SDS-polyacrylamide gel (7–9). First, we examined the contribution of several serine/threonine kinases and tyrosine kinases to this band shift with specific inhibitors against phospholipase C (U73122), PKC (Gö6983), PI3K

[4] Y. Kamioka, S. Yasuda, Y. Fujita, K. Aoki, and M. Matsuda, unpublished data.

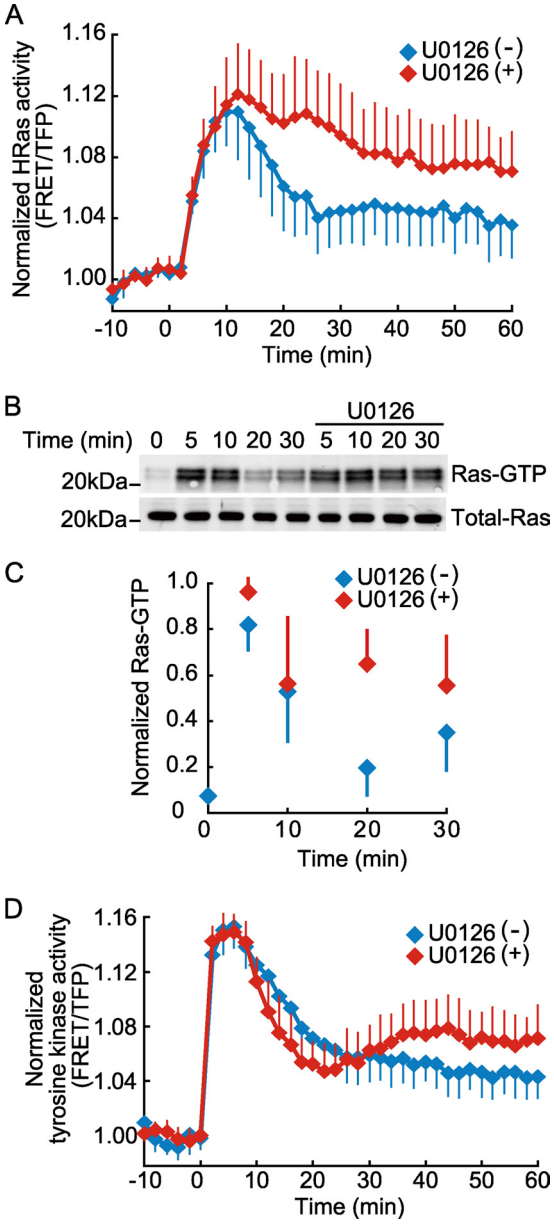

FIGURE 1. **ERK-mediated negative feedback loop to Ras.** *A*, Ras activity was monitored in HeLa cells stably expressing the Raichu-HRas FRET biosensor. The net intensities of TFP and FRET in each cell were measured, and the average emission ratio (FRET/TFP) was calculated. The FRET efficiency was normalized by the average value before stimulation. Cells were starved for 3 h and pretreated with the MEK inhibitor U0126 at a concentration of 10 μM for 10 min or untreated before addition of 10 ng/ml EGF at time point 0. The averages of the normalized FRET/TFP ratios obtained in the absence and presence of U0126 are shown in *blue* ($n = 14$) and *red* ($n = 12$), respectively. *B*, HeLa cells were serum-starved, pretreated with 10 μM U0126 for 10 min or untreated, and stimulated with 50 ng/ml EGF for the indicated periods. Ras-GTP levels in the cells were analyzed by Bos and co-workers' (22) pulldown method with the GST-tagged Ras-binding domain of cRaf. The amount of Ras-GTP collected was quantified with an Odyssey Imager system. The amount of Ras-GTP was normalized to the total Ras and plotted against time in *C*. *D*, tyrosine kinase activity was monitored in HeLa cells stably expressing the FRET biosensor Picchu. The averages of the normalized FRET/TFP ratios obtained in the absence and presence of U0126 are shown in *blue* ($n = 14$) and *red* ($n = 12$), respectively. *Error bars* indicate the S.D.

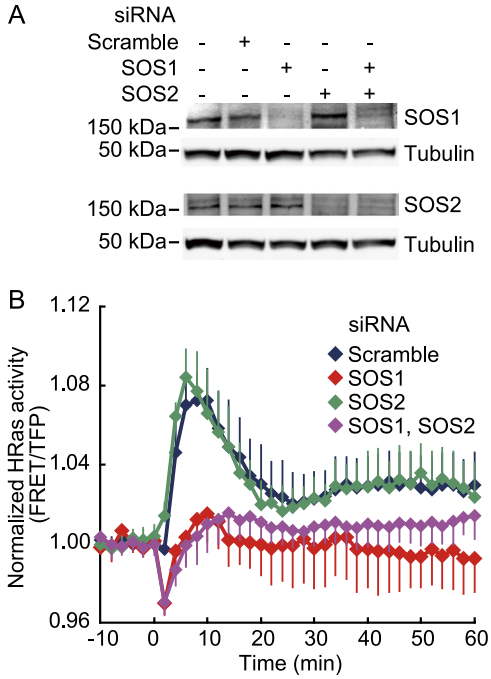

FIGURE 2. **Identification of SOS1 as primary GEF responsible for EGF-induced Ras activation in HeLa cells.** *A*, HeLa cells were transfected with siRNA against SOS1 and/or SOS2. Two days after transfection, the cells were lysed and analyzed by immunoblotting. Tubulin was used as a loading control. *B*, HeLa cells expressing Raichu-HRas were transfected with siRNA as in *A* and analyzed as described in Fig. 1. Thirteen cells were analyzed under each condition, and the averages and errors are shown. *Error bars* indicate the S.D.

(LY294002), MEK (U0126), p38 mitogen-activated protein kinase (SB203580), and Src (PP2). Among them, only U0126 could suppress the band shift of SOS1 induced by EGF (Fig. 3*A*). Assuming that the amount of the band shift correlates with the quantity of SOS1 phosphorylation, we compared the time courses of phosphorylation of EGFR, SOS1, and ERK (Fig. 3, *B-D*). We observed that phosphorylation of ERK increased rapidly, reached its zenith at 3 min, and decreased to less than 40% of the maximum activity within 30 min. In contrast, phosphorylation of SOS1 reached its zenith at 10 min after EGF stimulation and continued for 30 min. We calculated the dephosphorylation rate of SOS1 to be 0.0025/s by approximating the decay of phosphorylated SOS1 after acute ablation of MEK activity (Fig. 3, *E* and *F*) to the first-order kinetics as described under "Experimental Procedures." This half-life of phosphorylation, 4.6 min, is markedly faster than that used in the previous model (15) in which the dephosphorylation velocity and molecule number of SOS1 were 75 molecules/cell/min and 4×10^4 molecules/cell, respectively.

Suppression of EGF-induced Ras Activation and SOS1 Phosphorylation by Preactivated ERK—To confirm that ERK activation was sufficient for both suppression of Ras activity and phosphorylation of SOS1, we used a rapamycin-inducible cRaf translocation system (Fig. 4*A*) (21). The rapamycin-induced plasma membrane translocation of cRaf caused ERK activation and SOS1 phosphorylation as expected (Fig. 4*B*). This rapamycin-induced activation of cRaf markedly attenuated EGF-dependent Ras activation (Fig. 4*C*). Activation of EGFR as measured by the Picchu probe was not affected by the rapamycin-induced ERK activation (Fig. 4*D*). These results indicated that ERK activation was sufficient for the SOS1 phosphorylation and resulting inhibition of EGF-induced Ras activation. This result also showed that SOS1 could be phosphorylated by

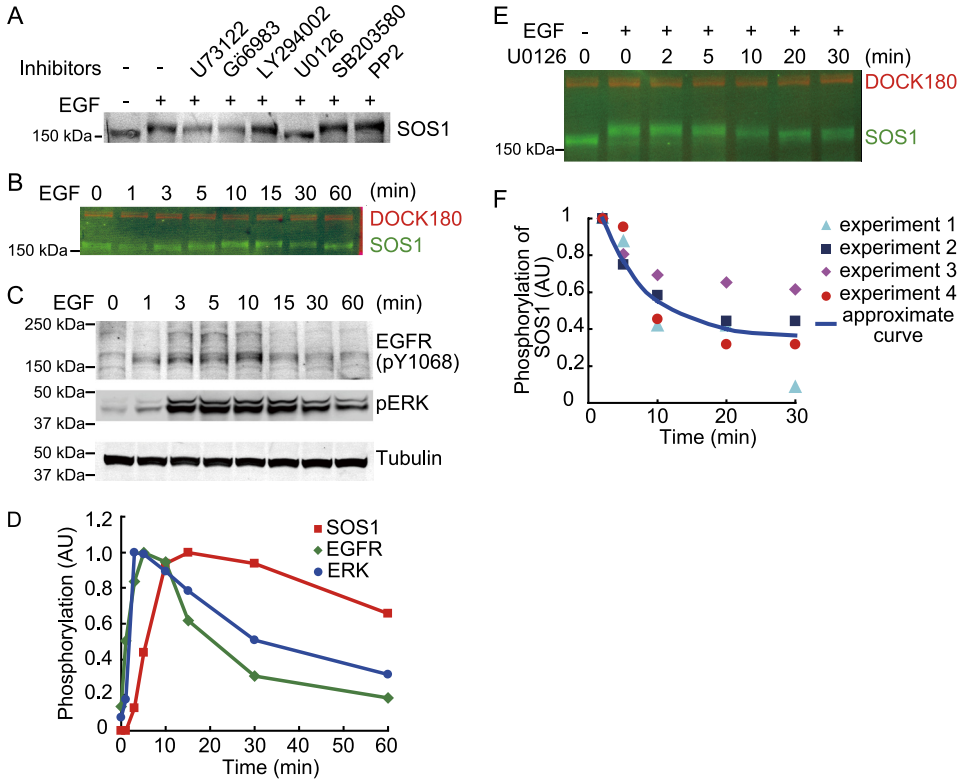

FIGURE 3. **Quantification of phosphorylation status of SOS1 by band shift in SDS-PAGE.** *A*, HeLa cells were starved for 3 h, pretreated with inhibitors for 10 min or untreated, and stimulated with 50 ng/ml EGF for 10 min or left unstimulated. Inhibitors were as follows: 10 μM U73122 for phospholipase C, 1 μM Gö6983 for PKC, 10 μM LY294002 for phosphatidylinositol 3-kinase, 10 μM U0126 for MEK, 10 μM SB203580 for p38 mitogen-activated protein kinase, and 10 μM PP2 for Src. Cells were lysed, separated by SDS-PAGE, and probed with an anti-SOS1 antibody. *B*, HeLa cells were starved and stimulated as in *A* for the indicated periods. The cell lysates were mixed with a standard protein, FLAG-DOCK180, and analyzed by immunoblotting with anti-FLAG mouse antibody and anti-SOS1 rabbit antibody, which were detected with anti-mouse IRDye 680 antibody and anti-rabbit IRDye 800 antibody, respectively. *C*, HeLa cells were starved and stimulated as in *B*. The cell lysates were analyzed by immunoblotting with EGFR (Tyr(P)-1068) antibody, anti-phospho-ERK (Tyr(P)-202/Tyr(P)-204) antibody, or anti-tubulin antibody. Tubulin was used as an internal loading control. *D*, the distance between FLAG-DOCK180 and SOS1 on the filter was measured, normalized to the maximum value, and plotted against time. The phosphorylation levels of ERK shown in *C* were also normalized to the maximum values and plotted. *E* and *F*, HeLa cells were starved for 3 h and stimulated with 50 ng/ml EGF for 10 min followed by the addition of 10 μM U0126 for the indicated periods. The band shift of SOS1 was quantified as in *D* and plotted against time ($n = 4$). *AU*, arbitrary units; *pERK*, phospho-ERK.

ERK in the absence of association with EGFR at the plasma membrane, which is a phosphotyrosine-dependent process.

Prediction of Role of Multiple SOS1 Phosphorylation Sites on Ras Activation—Based on these observations, we developed a kinetic simulation model of the ERK signaling pathway and examined the role of SOS1 phosphorylation *in silico*. We reported previously a kinetic simulation model of Ras-induced activation of ERK based on parameters determined experimentally (14). In the present study, we added EGFR and SOS1 to this model (supplemental Fig. S2). The concentrations of EGFR and SOS1 were determined by quantitative immunoblotting (supplemental Fig. S3). All parameters, including those related to SOS1 phosphorylation, are listed in supplemental Tables S1 and S2. In this model, four ERK-dependent phosphorylation sites in SOS1 were included based on the findings of a previous report (9).

The first question addressed in this work is whether phosphorylation of multiple sites is required to suppress SOS1 activity or a single phosphorylation of only one of the four sites is sufficient to suppress SOS1 activity. For simplicity, we classified phosphorylation sites into two types: a "relevant site" that regulates the SOS1 activity and an "irrelevant site" that does not regulate SOS1 activity. For the sake of simplicity, each SOS1 molecule was assumed to exhibit 100 or 0% activity depending on the phosphorylation status. With these simplifications, we built two models. In the first "cooperative" model, two to four relevant sites have to be phosphorylated to suppress SOS1 activity, whereas in the second "decisive" model, phosphorylation of any of the relevant phosphorylation site(s) is sufficient to suppress SOS1 activity.

The possible combinations of the SOS1 phosphorylation and the ratio of active and inactive SOS1 proteins in each model are schematically shown in Fig. 5. We offer triphosphorylated SOS1 as an example (Fig. 5, shown as *p3*). In the four-cooperative site model shown in Fig. 5, *top column*, all triphosphorylated SOS1 are active. In the three-cooperative site and two-cooperative site models, 75 and 50% of triphosphorylated SOS1 are active, respectively (the *second* and *third columns*). Meanwhile, 25% of triphosphorylated SOS1 is active in one-decisive site model (the *fourth column*), and none of the triphosphorylated SOS1 is active in the other decisive models.

We constrained these models by two of the experimental observations schematically shown in Fig. 6*A*. First, the duration of the EGF-induced activation of Ras was limited to less than 30 min to reproduce the transient Ras activation (Fig. 6*A*). Second, the basal level of phosphorylated SOS1 (pSOS) was assumed to be less than 25% (Fig. 6*A*). Unlike previous studies that contain only one species of GEF, this constraint became very important in our study because the basal ERK activity was maintained by a GEF other than SOS1. Under these constraints, we searched for parameter ranges of the K_m and k_{cat} of ERK-catalyzed phosphorylation of SOS1. K_m varied from 0.1 to 10 μM based on the K_m values of known ERK substrates (supplemental Table S3) (27–29). None of the cooperative models had solutions that fulfilled the aforementioned constraints. The k_{cat}/K_m value that reproduces transient Ras activation is much higher than that holding the basal level of pSOS to less than 25%.

Next we tested decisive models with one to four relevant phosphorylation sites; *i.e.* in these models, phosphorylation of any of the critical sites shut off the SOS1 activity. In each panel of Fig. 6*B*, the *yellow* region denotes the condition that phos-

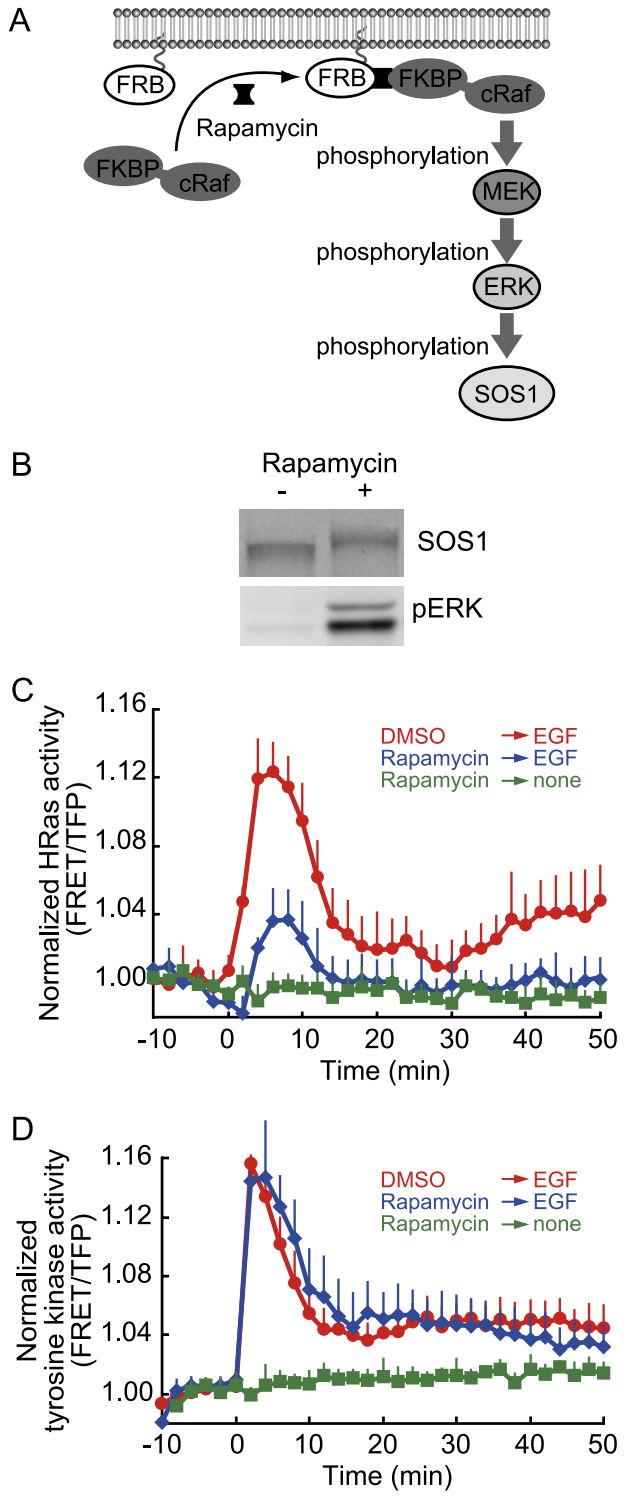

FIGURE 4. **Suppression of EGF-induced Ras activation by direct activation of ERK.** *A*, schematic representation of the rapamycin-inducible ERK activation system. The FKBP-cRaf fusion protein consists of the cRaf protein and the rapamycin-binding domain of FKBP12, indicated as *FKBP*. A protein indicated as *FRB* is an FK506-rapamycin-binding domain of mTOR fused to the myristoylation signal of Lyn. Upon rapamycin treatment, FKBP-tagged cRaf is recruited to the plasma membrane. The plasma membrane-recruited cRaf triggers sequential phosphorylation of MEK and ERK, which in turn phosphorylate SOS1 at multiple serine/threonine residues. *B*, ERK was directly activated in HeLa cells expressing cRaf-FKBP and LDR by the addition of 50 nM rapamycin for 10 min. Cell lysates were subjected to immunoblotting analysis with anti-SOS1 antibody or phospho-ERK (*pERK*) antibody. *C* and *D*, HeLa cells expressing Raichu-HRas (*C*) or Picchu (*D*) and the rapamycin-inducible cRaf translocation system were serum-starved for 3 h, incubated with DMSO or 50 nM rapamycin for 10 min, and stimulated with 50 ng/ml EGF or left unstimulated. Ras and tyrosine kinase activities were measured as in Fig. 1.

phorylation of basal SOS1 is less than 25%, and the *blue* region denotes the condition that the duration of EGF-stimulated Ras activation is less than 30 min. We found that these two regions overlapped in the very limited area shown in *green* in Fig. 6*B*. In particular, if we assume that K_m is over 1 μM as reported previously (27–29), only the model in which all of the four phosphorylation sites were critical could account for the observed combination of K_m and k_{cat}. Notably, the k_{cat} values expected in this model are much smaller than the k_{cat} values determined *in vitro* (supplemental Table S3), suggesting that the slow kinetics may be important for the negative feedback loop.

The role of the four critical phosphorylation sites in the decisive model was more intuitively illustrated by holding the K_m and k_{cat} values constant (Fig. 7). As the number of critical phosphorylation sites in the decisive model increased, the strength of the negative regulation increased as well. Importantly, the number of phosphorylation sites did not affect the rate or the strength of any of the signaling components in the activation phase.

Evaluation of Decisive Phosphorylation Model by Ablation of Negative Feedback Loop—To validate the model, we compared the dynamics of Ras activation between the *in silico* and the tissue culture conditions (Fig. 8). In the absence of the MEK inhibitor U0126, transient activation of Ras as observed in tissue culture was reproduced *in silico* with a wide range of EGF concentrations (Fig. 8, *A* and *C*). When the negative feedback loop was ablated by the MEK inhibitor, Ras activation was sustained both in tissue culture and *in silico* (Fig. 8, *B* and *D*). Interestingly, at high EGF concentrations, the suppression of Ras activity could not be completely restored as expected from the model (Fig. 8, *B* and *D*). This observation suggests the presence of another mechanism that attenuates the Ras activity after 10 min. It is likely that EGFR activity may be suppressed by endocytosis at high EGF concentration. This inability to reproduce the effect of U0126 at high EGF concentration is a flaw of the present model; however, in other words, this observation clearly indicates that our model based on the experimentally verified parameters could let us know that a critical regulator is missing in our knowledge.

DISCUSSION

In this study, we attempted to incorporate a negative feedback loop from ERK to SOS into our previously developed kinetic simulation model based on the experimentally verified parameters (14). In the EGF-ERK signaling cascade, there are many negative feedback loops, the effects of which sometimes depend on the cell type and/or cellular context (13, 30). In the early phase within 1 h after EGF stimulation, ERK-dependent phosphorylation of SOS1 plays a major role in the negative feedback regulation of this signaling cascade in many cell types (7–12, 31) as well as in the HeLa cells used in this study (Figs. 1–3).

Previous tryptic phosphopeptide map analyses have revealed that EGF induces phosphorylation of several serine/threonine

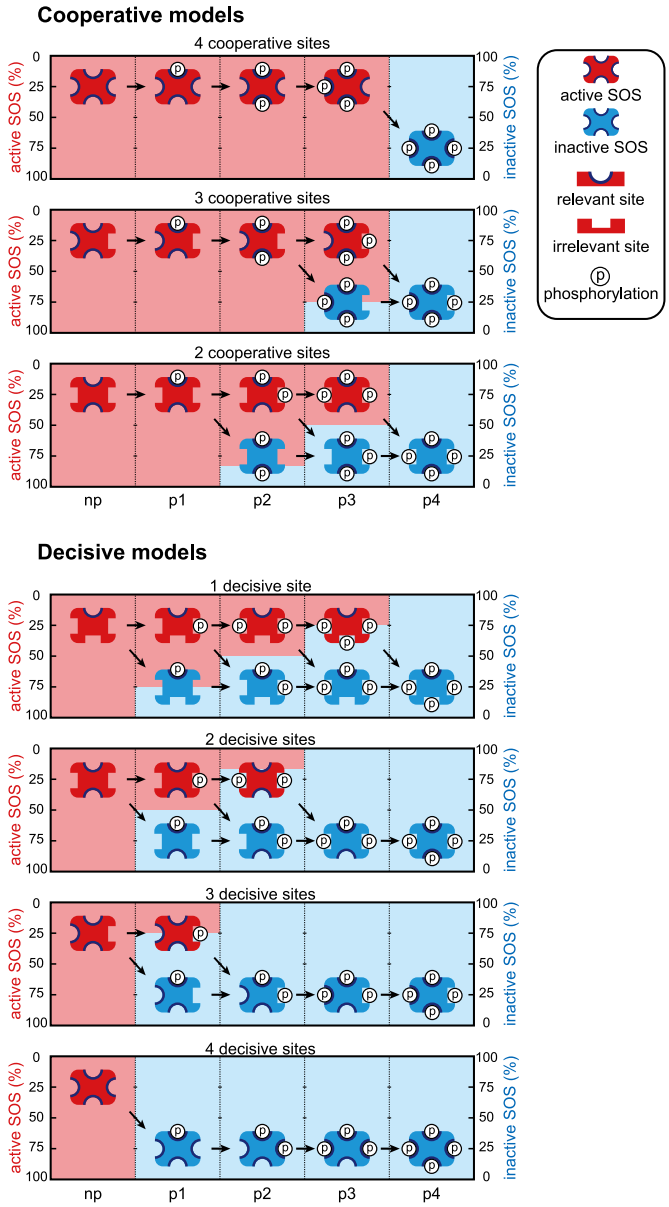

FIGURE 5. **Cooperative and decisive models for role of multiple phosphorylation sites on activity of SOS1.** To understand the role of multiple phosphorylations, we first classified phosphorylation sites into two types: a relevant site that regulates the SOS1 activity and an irrelevant site that does not regulate SOS1 activity. These two types of phosphorylation site are discriminated by *round* and *rectangular concave* symbols in this figure. For the sake of simplicity, each SOS1 molecule was assumed to exhibit 100 or 0% activity. The activities of SOS are depicted by either *red* or *blue* color of the symbols. Two models, the cooperative and decisive models, are considered according to the role of the phosphorylation sites. In the cooperative models, all critical phosphorylation sites have to be phosphorylated to suppress SOS1 activity, whereas in the decisive models, phosphorylation of any of the relevant sites is sufficient to suppress SOS1 activity. In both models, irrelevant phosphorylation sites do not affect the activity of SOS1 in any way. The *pink* and *blue background* colors show the ratio of active and inactive SOS1 proteins in each phosphorylation status (unphosphorylated (*np*), monophosphorylated (*p1*), diphosphorylated (*p2*), triphosphorylated (*p3*), or tetraphosphorylated (*p4*)) when the probability of the phosphorylation is equal among the four phosphorylation sites.

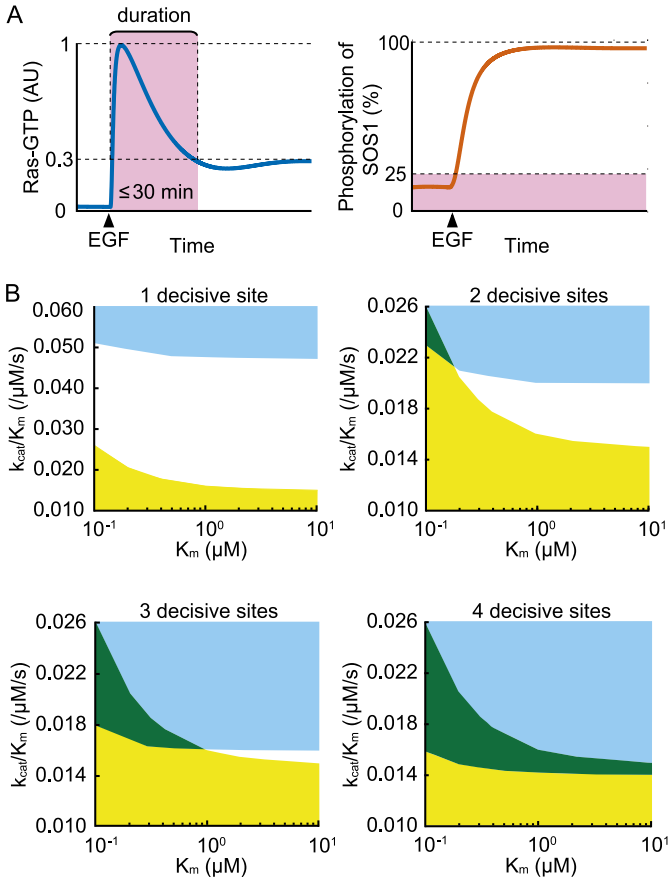

FIGURE 6. **Range of kinetic parameters constrained by duration of Ras activation and level of basal phosphorylation of SOS1.** *A*, schematic representation of the constraint for the parameters. The duration, which is defined as the period during which Ras activity is at least 30% of maximum, is restricted to less than 30 min to reproduce the transient activation *in vivo* (*left panel*). Phosphorylated SOS1, which is caused by basal ERK activity, is less than 25% of total SOS1 (*right panel*). *B*, range of K_m and k_{cat} of the ERK phosphorylation of SOS1 that fulfills the two constraints. The K_m and k_{cat} values are varied from 0.1 to 10 μM and from 0.001 to 1/s, respectively. The k_{cat}/K_m value is plotted against K_m. The regions that fulfill the constraints of transient Ras activation and basal ERK activity in *A* are indicated by *blue* and *yellow*, respectively. The overlapped regions are shown in *green*. *AU*, arbitrary units.

residues in the C-terminal region of human or murine Sos1 (8, 12). This C-terminal region contains multiple proline-rich motifs that bind to Grb2 (8); however, the phosphorylation of Sos1 does not affect Sos1 binding to Grb2 but perturbs Sos1 binding to Shc and EGFR (8, 12). Interestingly, serum- or insulin-induced phosphorylation of Sos1, which is also ERK-dependent, dissociates Sos1 from Grb2 (9–11). To accommodate this discrepancy in the role of Sos1 phosphorylation, we regarded SOS1 as representative of the SOS1-Grb2-Shc complex, which is dissociated from EGFR in an SOS1 phosphorylation-dependent manner in the present simulation model.

A specific question addressed in the present study is the role of the cluster of phosphoserine residues in the EGF-stimulated SOS1 protein. Corbalan-Garcia *et al.* (9) have reported that mutation of these phosphorylation sites renders the SOS1 protein insensitive to phosphorylation dependent-dissociation from Grb2. The same phosphorylation-defective mutant of SOS1 has been shown to be insensitive to ERK-mediated negative regulation in basic fibroblast growth factor-stimulated NIH-3T3 cells (32). However, to the best of our knowledge, there is no report examining the role of each phosphorylation site of SOS1. In addition, it is unknown whether SOS1 activity is

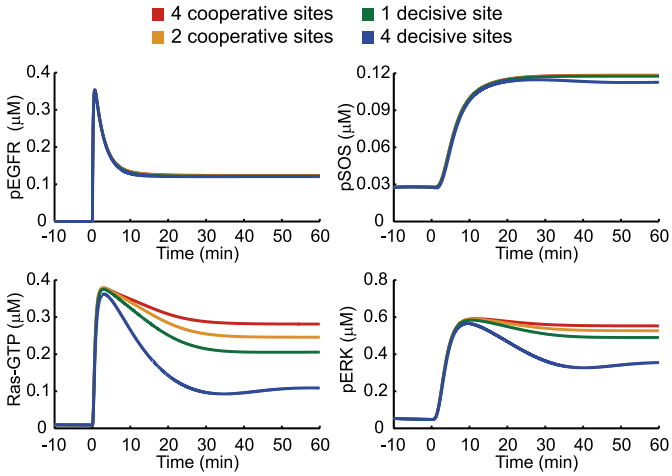

FIGURE 7. **Kinetics of signaling molecules with different numbers of cooperative or decisive phosphorylation sites.** The patterns of phospho-EGFR (*pEGFR*), pSOS, Ras-GTP, and phospho-ERK (*pERK*) were simulated in the decisive models according to Fig. 5. K_m = 5 μM; k_{cat} = 0.07/s; EGF, 50 ng/ml.

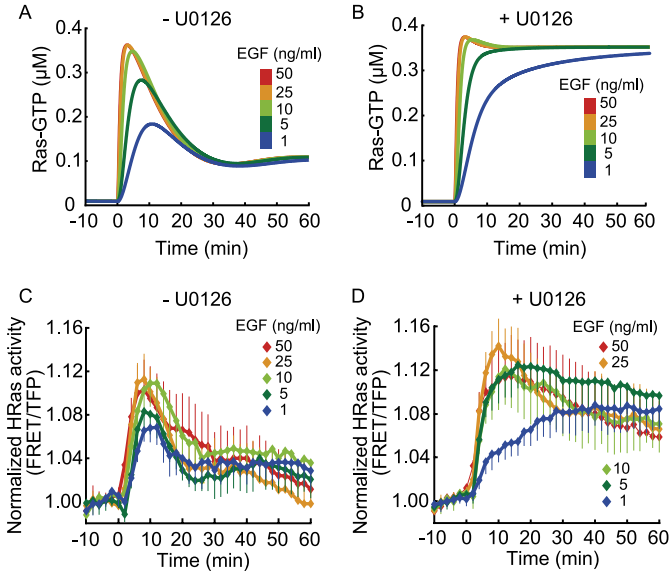

FIGURE 8. **Reproduction of effect of MEK inhibitor by kinetic simulation model of EGF-ERK pathway including negative feedback loop to SOS1.** *A* and *B*, the amount of Ras-GTP in EGF-stimulated cells was calculated at various EGF concentrations and plotted against time. MEK activity was ablated in the model shown in *B*. K_m = 5 μM, k_{cat} = 0.07/s. *C* and *D*, HeLa cells expressing Raichu-HRas were serum-starved for 3 h, pretreated with 10 μM U0126 for 10 min (*D*) or untreated (*C*), and stimulated with various concentrations of EGF as indicated. The Ras activity was monitored as described in Fig. 1. The numbers of samples are as follows: 1 ng/ml EGF, n = 12; 5 ng/ml EGF, n = 14; 10 ng/ml EGF, n = 14; 25 ng/ml EGF, n = 14; 50 ng/ml EGF, n = 14.

regulated by each phosphorylation site in a decisive manner or by multiple phosphorylation sites in a cooperative manner.

There are several previous examples of protein functions that are regulated by a cluster of serine and/or threonine phosphorylation within a relatively small region. The *Drosophila* clock protein Period is heavily phosphorylated in the per-short domain and per-short downstream domain, which together encompass some 60 amino acids in length. This hyperphosphorylation is associated with short period circadian rhythms and the stability of Period (33). Another example is the retinoblastoma tumor suppressor protein (RB). In its hypophosphorylated state, RB sequesters a subset of E2F complexes. Cdk-dependent hyperphosphorylation of RB dissociates E2F from RB, thereby triggering cell cycle-related genes (34, 35). In these previous studies, the contribution made by the phosphorylation of each specific amino acid residue was examined with mutants having a single amino acid substitution. However, as is the case with SOS1, it is largely unknown whether multiple phosphorylation sites regulate the protein function decisively or cooperatively in either Period or RB.

In this study, instead of experimentally examining the contribution of each phosphorylation site one by one, we built various kinetic simulation models and tested their probability *in silico* (Figs. 5 and 6). We constrained these models by two conditions. First, the amount of pSOS before stimulation was restricted to less than 25% of total SOS (Constraint 1). This condition was based on our own observation and also on previous tryptic mappings of pSOS before and after EGF stimulation (8, 12). Second, EGF-stimulated Ras activation was constrained to return to the near basal level within 30 min (Fig. 1). To our surprise, these two conditions rejected most of the models and left only one model in which all four phosphorylation sites play the decisive role in the negative regulation of SOS1 (Fig. 6). In other words, the model predicted that single phosphorylation of SOS1 was sufficient to dissociate SOS1 from EGFR. This role of multiple phosphorylation sites is similar to that of rhodopsin (36). Rhodopsin is phosphorylated at multiple sites in the C-terminal region upon photon absorption. Each phosphorylation site independently inactivates rhodopsin, thereby conferring reproducibility in single photon response. Therefore, the multiple decisive phosphorylation sites may be used in a variety of signal transduction modules to increase the fidelity of signaling.

Lastly, we should consider the reason why previous simulation models were able to reproduce the ERK-dependent suppression of SOS1 without taking the multiple phosphorylation sites into consideration. Three critical differences between these previous reports and the present study are schematically shown in supplemental Fig. S4. First, Brightman and Fell (15), whose model of the negative feedback loop from ERK to SOS has been adopted in many studies, postulated that ERK phosphorylates only SOS in complex with EGFR but not SOS in the cytoplasm (supplemental Fig. S4B). Because in this model ERK does not phosphorylate SOS1 in the basal state, the parameters that govern the phosphorylation of SOS1, K_m and k_{cat}, or the dephosphorylation rate of pSOS can be selected without the constraint of less than 25% pSOS in the basal state (Constraint 1). This assumption, however, was negated by the direct activation of cRaf, which resulted in efficient SOS1 phosphorylation and inactivation, indicating that ERK phosphorylates SOS1 irrespective of the localization (Fig. 4).

Second and most importantly, the basal level of active ERK was neglected in all preceding models (15, 17, 37) (supplemental Fig. S4C). This assumption also clears the constraint of less than 25% pSOS in the basal state.

Third, the parameter values concerning the phosphorylation and dephosphorylation of SOS1 in the previous models were sometimes significantly different from ours. For example, the half-life of pSOS was about 3 h in the model of Brightman and

Fell (15). In this way, negative feedback of SOS could be made almost irreversible in the time range used. However, as we show in Fig. 3, pSOS is rapidly dephosphorylated by phosphatases, indicating that the pSOS level is balanced by phosphorylation and dephosphorylation cycles.

The present model contained two major modifications, EGF-induced SOS1 activation and ERK phosphorylation of SOS1, and several updates of parameters in comparison with the previous model (14). To examine the effect of such modifications, we conducted sensitivity analysis (supplemental Fig. S5). The transient Ras activation (Constraint 1) was most sensitively influenced by the rate of ERK phosphorylation of SOS and also by the concentration of ERK. The basal low SOS1 phosphorylation (Constraint 2) was modestly affected by many parameters. Our simulation model consists of minimum number of reactions; therefore, perturbation in most parameters linearly affects the output such as SOS1 phosphorylation. Acquisition of experimentally verified parameters and the refinement of the model may yield a more robust model, or this system is inherently sensitive to many kinetic parameters.

In conclusion, with the help of experimentally verified parameters and a simulation model, we have found that multiple decisive phosphorylation sites contribute to the suppression of SOS1. Because phosphoproteomics has revealed a number of phosphorylation sites in many other signaling molecules, multiple decisive phosphorylation sites similar to that of SOS1 may be identified in other proteins.

Acknowledgments—We thank A. Miyawaki, N. Gotoh, T. Akagi, and D. Bar-Sagi for provision of the plasmids. A. Nishiyama-Abe and Y. Kasakawa are also thanked for technical assistance. We are grateful to the members of the Matsuda Laboratory for helpful discussions.

REFERENCES

1. Murphy, L. O., and Blenis, J. (2006) *Trends Biochem. Sci.* **31,** 268–275
2. Katz, M., Amit, I., and Yarden, Y. (2007) *Biochim. Biophys. Acta* **1773,** 1161–1176
3. Bar-Sagi, D. (1994) *Trends Endocrinol. Metab.* **5,** 165–169
4. Gureasko, J., Galush, W. J., Boykevisch, S., Sondermann, H., Bar-Sagi, D., Groves, J. T., and Kuriyan, J. (2008) *Nat. Struct. Mol. Biol.* **15,** 452–461
5. Margarit, S. M., Sondermann, H., Hall, B. E., Nagar, B., Hoelz, A., Pirruccello, M., Bar-Sagi, D., and Kuriyan, J. (2003) *Cell* **112,** 685–695
6. Dikic, I. (2003) *Biochem. Soc. Trans.* **31,** 1178–1181
7. Waters, S. B., Yamauchi, K., and Pessin, J. E. (1995) *Mol. Cell. Biol.* **15,** 2791–2799
8. Rozakis-Adcock, M., van der Geer, P., Mbamalu, G., and Pawson, T. (1995) *Oncogene* **11,** 1417–1426
9. Corbalan-Garcia, S., Yang, S. S., Degenhardt, K. R., and Bar-Sagi, D. (1996) *Mol. Cell. Biol.* **16,** 5674–5682
10. Cherniack, A. D., Klarlund, J. K., Conway, B. R., and Czech, M. P. (1995) *J. Biol. Chem.* **270,** 1485–1488
11. Corbalan-Garcia, S., Degenhardt, K. R., and Bar-Sagi, D. (1996) *Oncogene* **12,** 1063–1068
12. Porfiri, E., and McCormick, F. (1996) *J. Biol. Chem.* **271,** 5871–5877
13. Orton, R. J., Sturm, O. E., Vyshemirsky, V., Calder, M., Gilbert, D. R., and Kolch, W. (2005) *Biochem. J.* **392,** 249–261
14. Fujioka, A., Terai, K., Itoh, R. E., Aoki, K., Nakamura, T., Kuroda, S., Nishida, E., and Matsuda, M. (2006) *J. Biol. Chem.* **281,** 8917–8926
15. Brightman, F. A., and Fell, D. A. (2000) *FEBS Lett.* **482,** 169–174
16. Hatakeyama, M., Kimura, S., Naka, T., Kawasaki, T., Yumoto, N., Ichikawa, M., Kim, J. H., Saito, K., Saeki, M., Shirouzu, M., Yokoyama, S., and Konagaya, A. (2003) *Biochem. J.* **373,** 451–463
17. Yamada, S., Taketomi, T., and Yoshimura, A. (2004) *Biochem. Biophys. Res. Commun.* **314,** 1113–1120
18. Kurokawa, K., Mochizuki, N., Ohba, Y., Mizuno, H., Miyawaki, A., and Matsuda, M. (2001) *J. Biol. Chem.* **276,** 31305–31310
19. Mochizuki, N., Yamashita, S., Kurokawa, K., Ohba, Y., Nagai, T., Miyawaki, A., and Matsuda, M. (2001) *Nature* **411,** 1065–1068
20. Akagi, T., Sasai, K., and Hanafusa, H. (2003) *Proc. Natl. Acad. Sci. U.S.A.* **100,** 13567–13572
21. Inoue, T., Heo, W. D., Grimley, J. S., Wandless, T. J., and Meyer, T. (2005) *Nat. Methods* **2,** 415–418
22. Franke, B., Akkerman, J. W., and Bos, J. L. (1997) *EMBO J.* **16,** 252–259
23. Aoki, K., Nakamura, T., Inoue, T., Meyer, T., and Matsuda, M. (2007) *J. Cell. Biol.* **177,** 817–827
24. Aoki, K., and Matsuda, M. (2009) *Nat. Protoc.* **4,** 1623–1631
25. Tachibana, M., Kiyokawa, E., Hara, S., Iemura, S., Natsume, T., Manabe, T., and Matsuda, M. (2009) *Exp. Cell. Res.* **315,** 863–876
26. Lockyer, P. J., Wennström, S., Kupzig, S., Venkateswarlu, K., Downward, J., and Cullen, P. J. (1999) *Curr. Biol.* **9,** 265–268
27. Jacobs, D., Glossip, D., Xing, H., Muslin, A. J., and Kornfeld, K. (1999) *Genes Dev.* **13,** 163–175
28. Zhou, B., and Zhang, Z. Y. (2002) *J. Biol. Chem.* **277,** 13889–13899
29. Matsuura, I., Wang, G., He, D., and Liu, F. (2005) *Biochemistry* **44,** 12546–12553
30. Bublil, E. M., and Yarden, Y. (2007) *Curr. Opin. Cell. Biol.* **19,** 124–134
31. Kiel, C., and Serrano, L. (2009) *Sci. Signal.* **2,** ra38
32. Nakayama, K., Satoh, T., Igari, A., Kageyama, R., and Nishida, E. (2008) *Curr. Biol.* **18,** R332–R334
33. Kivimäe, S., Saez, L., and Young, M. W. (2008) *PLoS Biol.* **6,** e183
34. Harbour, J. W., and Dean, D. C. (2000) *Genes Dev.* **14,** 2393–2409
35. Sherr, C. J. (1996) *Science* **274,** 1672–1677
36. Doan, T., Mendez, A., Detwiler, P. B., Chen, J., and Rieke, F. (2006) *Science* **313,** 530–533
37. Sasagawa, S., Ozaki, Y., Fujita, K., and Kuroda, S. (2005) *Nat. Cell Biol.* **7,** 365–373

Multiple Decisive Phosphorylation Sites for the Negative Feedback Regulation of SOS1 via ERK

Yuji Kamioka, Shuhei Yasuda, Yoshihisa Fujita, Kazuhiro Aoki and Michiyuki Matsuda

J. Biol. Chem. 2010, 285:33540-33548.
doi: 10.1074/jbc.M110.135517 originally published online August 19, 2010

Table S1 Concentration of signaling molecules in HeLa cells.

Species name	Concentration (μM)	Comments
EGF	0.0016	10 ng/ml
EGFR	0.42	Fig. S3
SOS1	0.12[a]	Fig. S3
Ras	0.43	Fujioka et al., 2006
RasGAP	1.0	Arbitrary.
RasGEF	1.0	Arbitrary.
RasEffector	2.0	Fujioka et al., 2006
Raf	0.013	Fujioka et al., 2006
MEK	1.4	Fujioka et al., 2006
ERK	0.96	Fujioka et al., 2006

(a) The sum of unphosphorylated SOS, pSOS, ppSOS, pppSOS, and ppppSOS is set to 0.12 μM.

Reference

Fujioka, A., Terai, K., Itoh, R. E., Aoki, K., Nakamura, T., Kuroda, S., Nishida, E., and Matsuda, M. (2006) *J. Biol. Chem.* **281**, 8917-8926

Table S2 **Kinetic reactions and parameters**.

Reaction #	Reaction and equation	Parameters			Comments
Re1	EGF + EGFR -> pEGFR kf_EGF_EGFR_binding * [EGF] * [EGFR]	kf_EGF_EGFR_binding	10	/μM/s	Estimated [a].
Re2	pEGFR <=> pEGFR_degra	kf_pEGFR_degradation	0.005	/s	Estimated [a].
	kf_pEGFR_degradation * [pEGFR] - kb_pEGFR_recycle * [pEGFR_degra]	kb_pEGFR_recycle	0.002	/s	Estimated [a].
Re3	pEGFR + SOS1 <=> pEGFR_SOS1	kf_SOS1_pEGFR_binding	0.1	/μM/s	Arbitrary [b].
	kf_SOS1_pEGFR_binding * [pEGFR] * [SOS1] - kb_SOS1_pEGFR_dissociation * [pEGFR_SOS1]	kb_SOS1_pEGFR_dissociation	0.1	/s	Arbitrary [b].
Re4	SOS1 + pERKcyt (enzyme) <=> pSOS	kcat_pERKcyt_SOS1	0.02	/s	See text.
	kcat_pERKcyt_SOS1 * [pERKcyt] * [SOS1] / (Km_pERKcyt_SOS1 + [SOS1]) - kdphos_pSOS_SOS1 * [pSOS]	Km_pERKcyt_SOS1	1	μM	See text.
		kdphos_pSOS_SOS1	0.0025	/s	Fig. 3*F*
Re5	RasGDP + pEGFR_SOS1 (enzyme) -> RasGTP Kf_SOS1_Ras * [pEGFR_SOS1] * [RasGDP]	kf_SOS1_Ras	1	/μM/s	Modified from Gureasko et al.,
Re6	RasGDP + RasGEF (enzyme) -> RasGTP kf_RasGEF * [RasGEF] * [RasGDP]	kf_RasGEF	0.00005	/μM/s	Estimated [c].
Re7	RasGTP + RasGAP (enzyme) -> RasGDP kf_RasGAP * [RasGAP] * [RasGTP]	kf_RasGAP	0.05	/μM/s	Estimated [c].
Re8	RasGTP + Effector <=> Ras_Effector	kf_Ras_Effector_binding	1	/μM/s	Estimated [d].
	kf_Ras_Effector_binding * [RasGTP] * [Effector] - kb_Ras_Effector_dissociation * [Ras_Effector]	kb_Ras_Effector_dissociation	0.1	/μM	Estimated [d].

Reaction #	Reaction and equation	Parameters			Comments
Re9	RasGTP + Raf <=> RasGTP_Raf	kf_Ras_Raf_binding	0.49	/μM/s	Fujioka et al., 2006
	kf_Ras_Raf_binding * [RasGTP] * [Raf] - kb_Ras_Raf_dissociation * [RasGTP_Raf]	kb_Ras_Raf_dissociation	0.049	/s	Fujioka et al., 2006
Re10	RasGTP_Raf + MEKcyt <=> RasGTP_Raf_MEK	kf_Raf_MEK_binding	0.65	/μM/s	Fujioka et al., 2006
	kf_Raf_MEK_binding * [RasGTP_Raf] * [MEKcyt] - kb_Raf_MEK_dissociation * [RasGTP_Raf_MEK]	kb_Raf_MEK_dissociation	0.065	/s	Fujioka et al., 2006
Re11	RasGTP_Raf_MEK -> RasGTP_Raf + pMEKcyt	kphos_MEK_pMEK	0.6	/s	Estimated [e].
	kphos_MEK_pMEK * [RasGTP_Raf_MEK]				
Re12	pMEKcyt -> MEKcyt	kdphos_pMEK_MEK	0.0096	/s	K. Aoki, unpublished
	kdphos_pMEK_MEK * [pMEKcyt]				
Re13	pMEKcyt + ERKcyt <=> pMEK_ERKcyt	kf_MEK_ERK_binding	0.18	/μM/s	K. Aoki, unpublished
	kf_MEK_ERK_binding * [pMEKcyt] * [ERKcyt] - kb_MEK_ERK_dissociation * [pMEK_ERKcyt]	kb_MEK_ERK_dissociation	0.27	/s	K. Aoki, unpublished
Re14	MEKcyt + ERKcyt <=> MEK_ERKcyt	kf_MEK_ERK_binding	0.18	/μM/s	K. Aoki, unpublished
	kf_MEK_ERK_binding * [MEKcyt] * [ERKcyt] - kb_MEK_ERK_dissociation * [MEK_ERKcyt]	kb_MEK_ERK_dissociation	0.27	/s	K. Aoki, unpublished
Re15	pMEK_ERKcyt -> pMEKcyt + pERKcyt	kphos_ERK_pERK	0.6	/s	Estimated [e].
	kphos_ERK_pERK * [pMEK_ERKcyt]				
Re16	pERKcyt -> ERKcyt	kdphos_pERK_ERK	0.00447	/s	K. Aoki, unpublished
	kdphos_pERK_ERK * [pERKcyt]				

Reaction #	Reaction and equation	Parameters			Comments
Re17	MEKnuc <=> MEKcyt	kexport_MEK	0.03	/s	K. Aoki, unpublished
	0.2 * kexport_MEK * [MEKnuc] - kimport_MEK * [MEKcyt]	kimport_MEK	0.0004	/s	K. Aoki, unpublished
Re18	pMEKnuc <=> pMEKcyt	kexport_pMEK	0.03	/s	K. Aoki, unpublished
	0.2 * kexport_pMEK * [pMEKnuc] - kimport_pMEK * [pMEkcyt]	kimport_pMEK	0.0004	/s	K. Aoki, unpublished
Re19	ERKcyt <=> ERKnuc	kexport_ERK	0.011	/s	K. Aoki, unpublished
	kimport_ERK * [ERKcyt] - 0.2 * kexport_ERK * [ERKnuc]	kimport_ERK	0.0023	/s	K. Aoki, unpublished
Re20	pERKcyt <=> pERKnuc	kexport_pERK	0.011	/s	K. Aoki, unpublished
	kimport_pERK * [pERKcyt] - 0.2 * kexport_pERK * [pERKnuc]	kimport_pERK	0.0023	/s	K. Aoki, unpublished
Re21	MEK_ERKnuc <=> MEK_ERKcyt	kexport_MEK_ERK	0.03	/s	K. Aoki, unpublished
	0.2 * kexport_MEK_ERK * [MEK_ERKnuc] - kimport_MEK_ERK * [MEK_ERKcyt]	kimport_MEK_ERK	0.0004	/s	K. Aoki, unpublished
Re22	pMEK_ERKnuc <=> pMEK_ERKcyt	kexport_MEK_ERK	0.03	/s	K. Aoki, unpublished
	0.2 * kexport_MEK_ERK * [MEK_ERKnuc] - kimport_MEK_ERK * [MEK_ERKcyt]	kimport_MEK_ERK	0.0004	/s	K. Aoki, unpublished
Re23	pMEKnuc -> MEKnuc	kdphos_pMEK_MEK	0.0096	/s	K. Aoki, unpublished
	0.2 * kdphos_pMEK_MEK * [pMEKnuc]				

Reaction #	Reaction and equation	Parameters			Comments
Re24	MEKnuc + ERKnuc <=> MEK_ERKnuc	kf_MEK_ERK_binding	0.18	/μM/s	K. Aoki, unpublished
	0.2 * (kf_MEK_ERK_binding * [MEKnuc] * [ERKnuc] - kb_MEK_ERK_dissociation * [MEK_ERKnuc])	kb_MEK_ERK_dissociation	0.27	/s	K. Aoki, unpublished
Re25	pMEKnuc + ERKnuc <=> pMEK_ERKnuc	kf_MEK_ERK_binding	0.18	/μM/s	K. Aoki, unpublished
	0.2 * (kf_MEK_ERK_binding * [pMEKnuc] * [ERKnuc] - kb_MEK_ERK_dissociation * [pMEK_ERKnuc])	kb_MEK_ERK_dissociation	0.27	/s	K. Aoki, unpublished
Re26	pMEK_ERKnuc -> pMEKnuc + pERKnuc	kphos_ERK_pERK	0.6	/s	Estimated [e].
	0.2 * kphos_ERK_pERK * [pMEK_ERKnuc]				
Re27	pERKnuc -> ERKnuc	kdphos_pERK_ERK	0.00447	/s	K. Aoki, unpublished
	0.2 * kdphos_pERK_ERK * [pERKnuc]				

Reference

Gureasko, J., Galush, W. J., Boykevisch, S., Sondermann, H., Bar-Sagi, D., Groves, J. T., and Kuriyan, J. (2008) *Nat. Struct. Mol. Biol.* **15**, 452-461

Fujioka, A., Terai, K., Itoh, R. E., Aoki, K., Nakamura, T., Kuroda, S., Nishida, E., and Matsuda, M. (2006) *J. Biol. Chem.* **281**, 8917-8926

Aoki K., Yamada M., Komatsu N., Yasuda S., and Matuda, M**.** Manuscript in submission.

Basis for the estimation of parameters:

(a) Parameters concerning EGFR stability were estimated to reproduce the tyrosine kinase activity monitored by a FRET biosensor Picchu (Fig. 1*D*).

(b) Association and dissociation rates of the EGFR-SOS1 complex was set arbitrary to yield 0.1 μM Kd constant.

(c) Basal activities of GEFs and GAPs for Ras were constrained to reproduce the basal ERK activity less than 5% and basal pSOS less than 25% (Fig. 3*D*).

(d) Parameters concerning Ras effectors other than Raf were estimated to reproduce the transient Ras activation (Fig. 1*A*).

(e) Phosphorylation rates of MEK and ERK were estimated to reproduce the time course of ERK activation (Fig. 3*D*).

Table S3 K_m and k_{cat} of ERK substrates.

ERK substrates	K_m (μM)	k_{cat} (/sec)	References
MBP	3.3±0.5	1.05	Jacobs et al., 1999
MBP	55±25	1.33	Robinson et al., 1996
MBP	4.2±0.8	10	Prowse et al., 2000
MBP	10±1.3	6.5	Zhou et al., 2002
MBP	5.1±1.0	Not shown	Matsuura et al., 2005
GST-ELK1(307-428)	1.5±0.5	1.67	Jacobs et al., 1999
GST-ELK1(307-428)	1.95±0.2	10.2	Zhou et al., 2002
GST-ELK1(307-428)	1.8±0.3	Not shown	Matsuura et al., 2005
GST-AOP (480-732)	0.7±0.3	1.33	Jacobs et al., 1999
GST-LIN1 (281-441)	0.8±0.05	0.67	Jacobs et al., 1999
GST-Smad3	11.8±2.3	Not shown	Matsuura et al., 2005

Reference

Jacobs, D., Glossip, D., Xing, H., Muslin, A. J., and Kornfeld, K. (1999) *Genes Dev.* **13**, 163-175

Robinson, M. J., Harkins, P. C., Zhang, J., Baer, R., Haycock, J. W., Cobb, M. H., Goldsmith, E. J. (1996) *Biochemistry* **35**, 5641–5646

Prowse, C. N., Hagopian, J. C., Cobb, M. H., Ahn, N.G., Lew, J. (2000) *Biochemistry* **39**, 6258-6266

Zhou, B., and Zhang, Z. Y. (2002) *J. Biol. Chem.* **277**, 13889-13899

Matsuura, I., Wang, G., He, D., Liu, F. (2005) *Biochemistry* **44**, 12546-12553

Supplemental Data

Fig. S1. Effect of MEK inhibition by siRNA and PD184352.
(A), HeLa cells were transfected with an siRNA against MEK1 and MEK2. Three days after transfection, the cells were lysed and analyzed by immunoblotting. siRNA against human MEK1 and MEK2 (MEK1/2 #1) and RNAi negative control duplex (Scramble) were purchased from Invitrogen. (B), HeLa cells expressing Raichu-HRas were transfected with siRNA as in (A) and analyzed as described in Fig. 1. Twelve cells were analyzed under each condition and the averages and errors are shown. Error bars indicate the s.d. (C), Representative phase contrast images of control and MEK1/2 knockdown cells. Scale bars, 20 μm. (D), Cells were pretreated or untreated with a MEK inhibitor U0126 or PD184352 at a concentration of 10 μM for 10 minutes. Twelve cells were analyzed under each condition and the averages and errors are shown. Error bars indicate the s.d.

Fig. S2. Overview of the ERK MAPK pathway simulation in this study.
Block diagram of the kinetic simulation model of the EGF-ERK signaling cascade. All parameters and reactions are described in Supplemental Table S1 and S2.

Fig. S3. Quantification of the number of molecules of EGFR and SOS1.
The number of molecules of EGFR and SOS1 was quantified in HeLa cells by two steps. First, the EGFP-tagged EGFR and SOS1 were expressed in HeLa cells. Cell lysates were diluted with lysis buffer and loaded on SDS-polyacrylamide gel along with GST-YFP of known concentration, followed by immunoblotting with anti-GFP antibody (A, E). The bound antibody was quantified with a fluorimager to obtain the calibration curves of GFP vs. anti-GFP (B, F). From these plots the concentrations of EGFP-tagged EGFR and SOS in cell lysates were calculated. Second, the diluted cell lysates were loaded on SDS-polyacrylamide gel along with various amounts of HeLa cell lysates, followed by immunoblotting with either anti-EGFR antibody (C) or anti-SOS1 antibody (G). The bound antibodies were quantified with a fluorimager to obtain the calibration curves of EGFR-EGFP vs. anti-EGFR (D) or SOS1 vs. anti-SOS1 (F). The concentration of EGFR and SOS1 were calculated from these calibration plots. Data indicated with asterisks(*) are not used for the quantification because the intensity of the bands was out of the linear range of the calibration plots.

Fig. S4. Schematic representation of the critical difference between the present and previous models.
Block diagrams of SOS phosphorylation by ERK in the present and previous models. Before EGF stimulation, each model takes only the blocks pasted with green into consideration. In the present model (A), basal level ERK activity and the resulting accumulation of pSOS are used to constrain K_m and the rate constant of SOS phosphorylation by ERK. In the other models, the basal amount of pSOS is zero because pERK in the basal state is neglected. Furthermore, in Brightman and Fell model, pERK can phosphorylate only SOS in complex with EGFR. This assumption also contributes to decrease pSOS.

Fig. S5. Effect of parameter changes on the two constraints.
The amounts of Ras-GTP, phosphorylated ERK, and phosphorylated SOS were simulated at the indicated time points on each condition, wherein the indicated parameter was changed to 1/1.5 or 1.5 folds of the

default value. The variance is shown by pseudocolor scale. In the right columns, the fulfillment of Contraint #1 (transient Ras activation, Fig. 6 *A* left) and #2 (basal low SOS1 phosphorylation, Fig. 6 *A* right) is shown with two symbols, o and x.

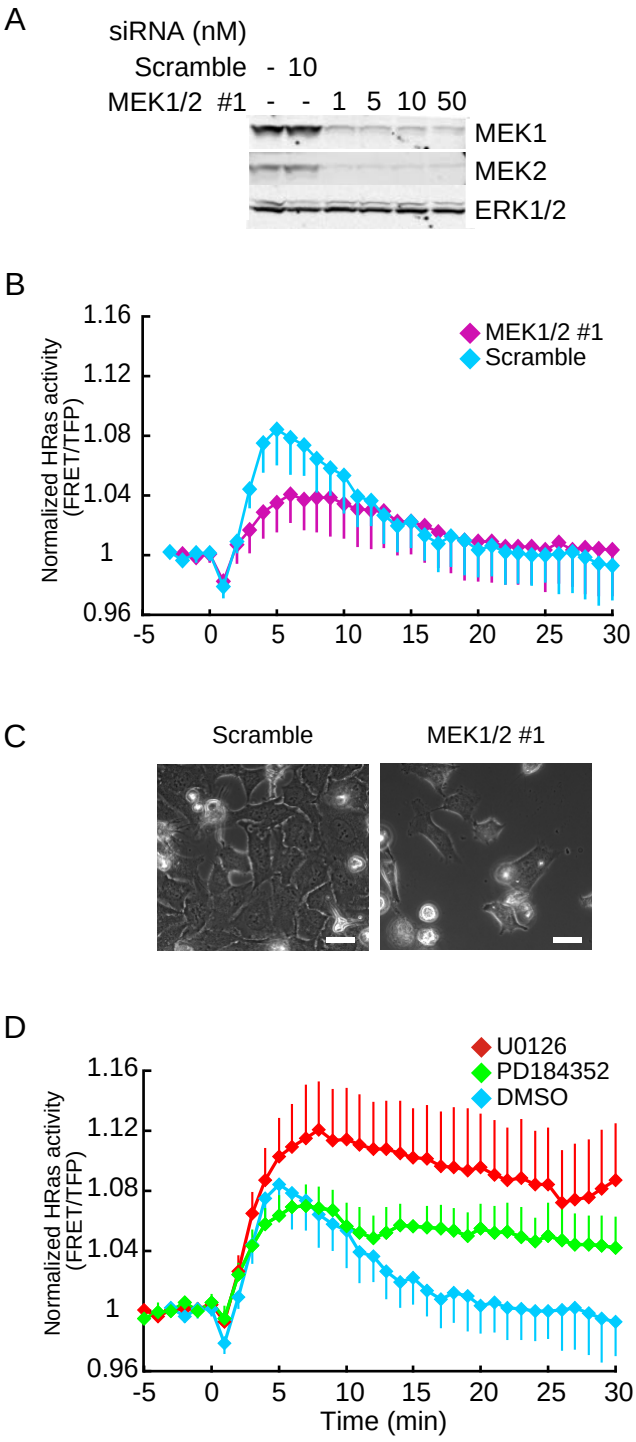
A
siRNA (nM)
Scramble - 10
MEK1/2 #1 - - 1 5 10 50
MEK1
MEK2
ERK1/2
B
MEK1/2 #1
Scramble
Normalized HRas activity (FRET/TFP)
1.16
1.12
1.08
1.04
1
0.96
-5 0 5 10 15 20 25 30
C
Scramble
MEK1/2 #1
D
U0126
PD184352
DMSO
Normalized HRas activity (FRET/TFP)
Time (min)

Fig. S1.

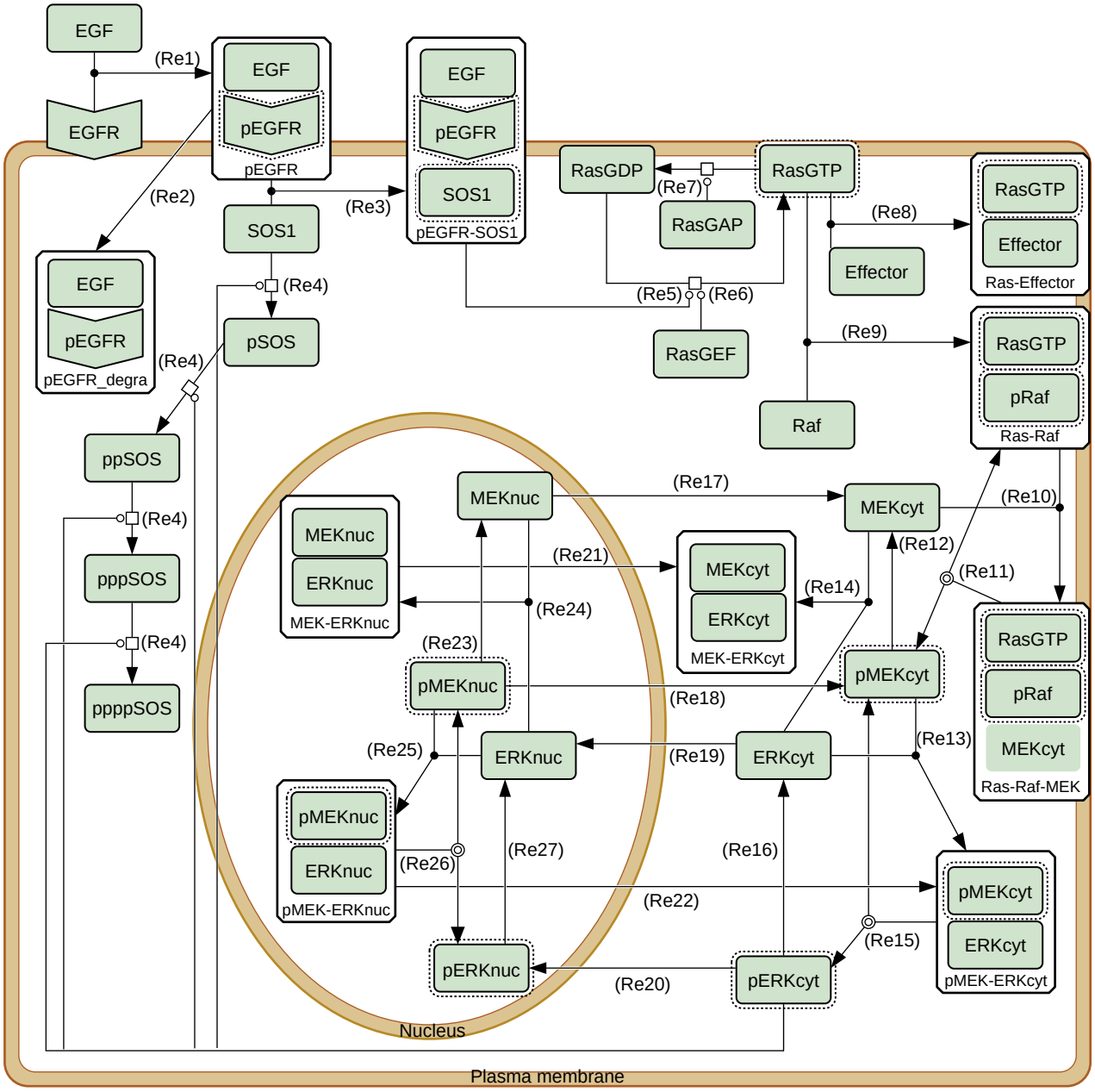
EGF
(Re1)
EGFR
EGF
pEGFR
pEGFR
(Re2)
(Re3)
SOS1
EGF
pEGFR
SOS1
pEGFR-SOS1
RasGDP
(Re7)
RasGTP
RasGAP
(Re8)
RasGTP
Effector
Effector
Ras-Effector
(Re5)
(Re6)
EGF
pEGFR
pEGFR_degra
(Re4)
pSOS
RasGEF
(Re9)
RasGTP
pRaf
Ras-Raf
Raf
(Re4)
ppSOS
(Re4)
pppSOS
(Re4)
ppppSOS
MEKnuc
(Re17)
MEKcyt
(Re10)
MEKnuc
ERKnuc
MEK-ERKnuc
(Re21)
MEKcyt
ERKcyt
MEK-ERKcyt
(Re12)
(Re11)
(Re14)
(Re24)
(Re23)
pMEKnuc
pMEKcyt
RasGTP
pRaf
MEKcyt
Ras-Raf-MEK
(Re18)
(Re25)
ERKnuc
(Re19)
ERKcyt
(Re13)
pMEKnuc
ERKnuc
pMEK-ERKnuc
(Re26)
(Re27)
(Re16)
(Re22)
pMEKcyt
ERKcyt
pMEK-ERKcyt
(Re15)
pERKnuc
(Re20)
pERKcyt
Nucleus
Plasma membrane

Fig. S2.

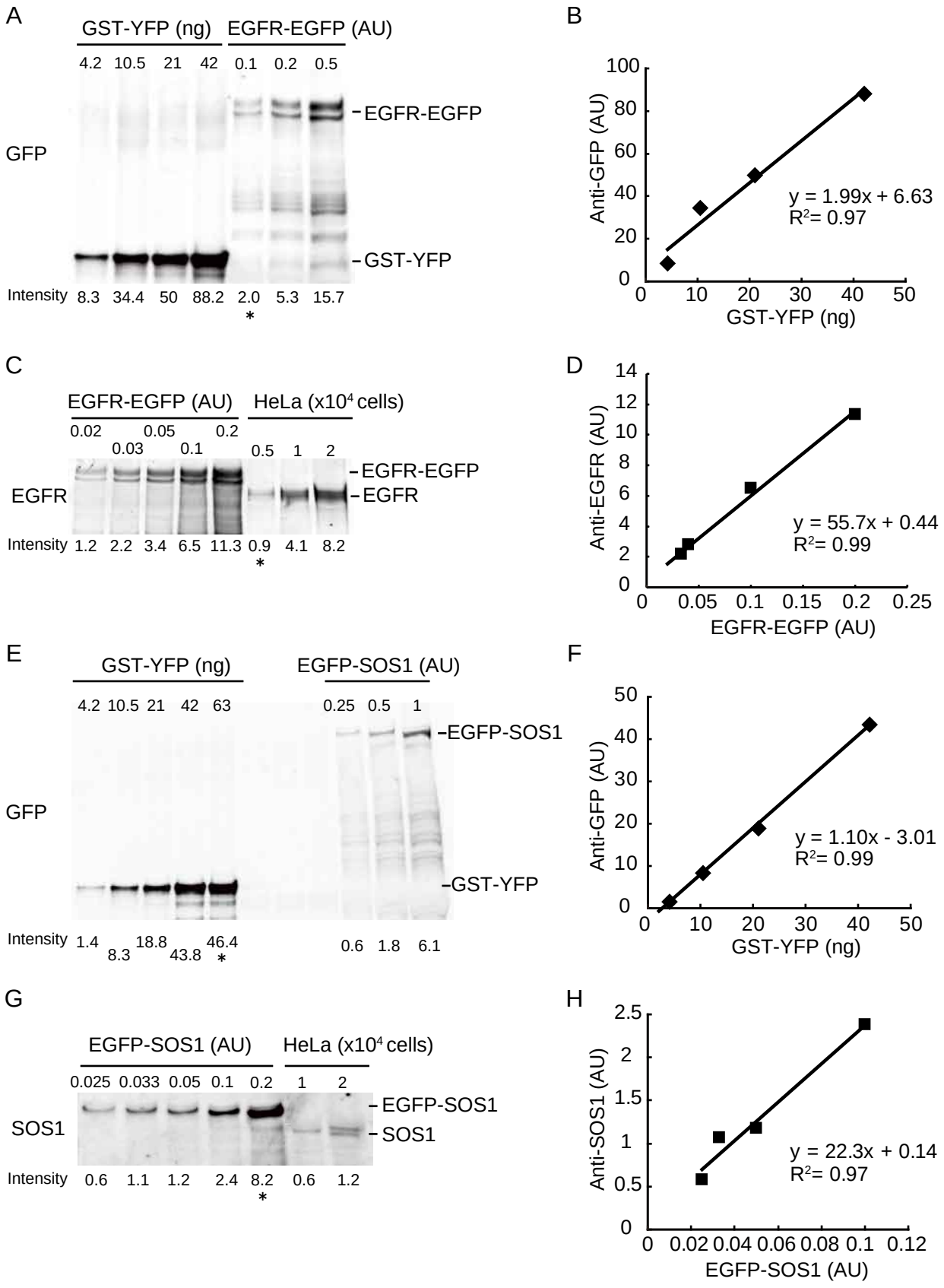
A
GST-YFP (ng)
EGFR-EGFP (AU)
4.2 10.5 21 42 0.1 0.2 0.5
GFP
EGFR-EGFP
GST-YFP
Intensity 8.3 34.4 50 88.2 2.0 5.3 15.7
*
B
Anti-GFP (AU)
GST-YFP (ng)
y = 1.99x + 6.63
R2= 0.97
C
EGFR-EGFP (AU)
HeLa (x10^4 cells)
0.02 0.05 0.2
0.03 0.1
0.5 1 2
EGFR
EGFR-EGFP
EGFR
Intensity 1.2 2.2 3.4 6.5 11.3 0.9 4.1 8.2
*
D
Anti-EGFR (AU)
EGFR-EGFP (AU)
y = 55.7x + 0.44
R2= 0.99
E
GST-YFP (ng)
EGFP-SOS1 (AU)
4.2 10.5 21 42 63
0.25 0.5 1
GFP
EGFP-SOS1
GST-YFP
Intensity 1.4 8.3 18.8 43.8 46.4 *
0.6 1.8 6.1
F
Anti-GFP (AU)
GST-YFP (ng)
y = 1.10x - 3.01
R2= 0.99
G
EGFP-SOS1 (AU)
HeLa (x10^4 cells)
0.025 0.033 0.05 0.1 0.2 1 2
SOS1
EGFP-SOS1
SOS1
Intensity 0.6 1.1 1.2 2.4 8.2 0.6 1.2
*
H
Anti-SOS1 (AU)
EGFP-SOS1 (AU)
y = 22.3x + 0.14
R2= 0.97

Fig. S3.

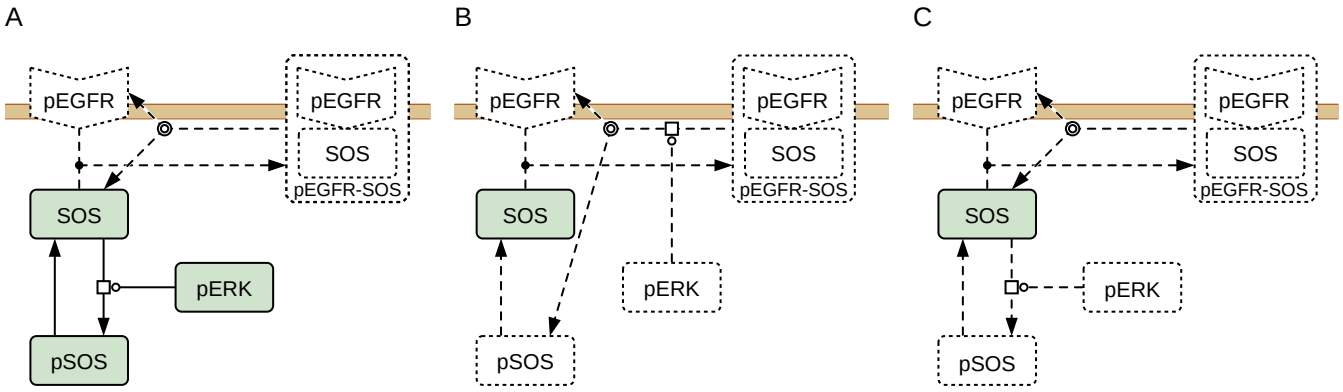

This study

Brightman and Fell

Yamada et al.
Sasagawa et al.

Fig. S4.

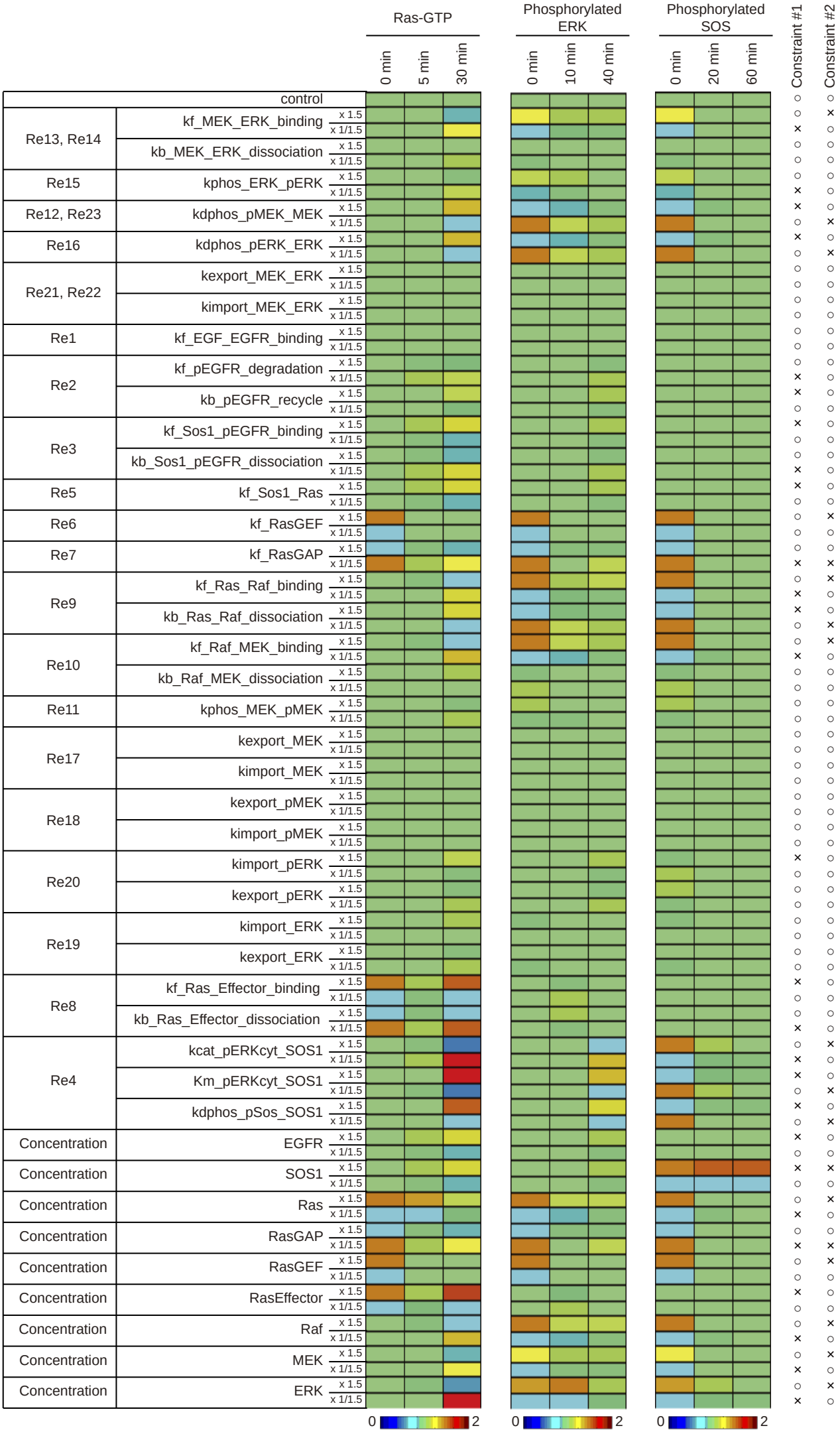
Ras-GTP
Phosphorylated ERK
Phosphorylated SOS
0 min
5 min
30 min
0 min
10 min
40 min
0 min
20 min
60 min
Constraint #1
Constraint #2
control
Re13, Re14
kf_MEK_ERK_binding
kb_MEK_ERK_dissociation
Re15
kphos_ERK_pERK
Re12, Re23
kdphos_pMEK_MEK
Re16
kdphos_pERK_ERK
Re21, Re22
kexport_MEK_ERK
kimport_MEK_ERK
Re1
kf_EGF_EGFR_binding
Re2
kf_pEGFR_degradation
kb_pEGFR_recycle
Re3
kf_Sos1_pEGFR_binding
kb_Sos1_pEGFR_dissociation
Re5
kf_Sos1_Ras
Re6
kf_RasGEF
Re7
kf_RasGAP
Re9
kf_Ras_Raf_binding
kb_Ras_Raf_dissociation
Re10
kf_Raf_MEK_binding
kb_Raf_MEK_dissociation
Re11
kphos_MEK_pMEK
Re17
kexport_MEK
kimport_MEK
Re18
kexport_pMEK
kimport_pMEK
Re20
kimport_pERK
kexport_pERK
Re19
kimport_ERK
kexport_ERK
Re8
kf_Ras_Effector_binding
kb_Ras_Effector_dissociation
Re4
kcat_pERKcyt_SOS1
Km_pERKcyt_SOS1
kdphos_pSos_SOS1
Concentration
EGFR
SOS1
Ras
RasGAP
RasGEF
RasEffector
Raf
MEK
ERK
x 1.5
x 1/1.5
0
2

Fig. S5.